

# Characterization of a turbulent flow with independent variation of Mach and Reynolds numbers

N. Manzano-Miura · D. Gloutak · G. P. Bewley

Received: date / Accepted: date

**Abstract** The Variable Density and Speed of Sound Vessel (VDSSV) produces subsonic turbulent flows that are compressible and in which turbulent fluctuations can be resolved at all scales with existing instrumentation including hot wires and particle tracking. We realize this objective by looking at the flow of a heavy gas (sulfur hexafluoride  $\text{SF}_6$ ), with a speed of sound almost three times lower than for air. By switching between air and  $\text{SF}_6$ , we isolate the influence of the turbulent Mach number (up to  $M_t = 0.17$ ) on turbulence statistics from the influences of changes in the Reynolds number (up to  $R_\lambda = 1600$ ), and boundary conditions, which we hold constant. A free shear flow is produced by a ducted fan, and we show that it behaves like a turbulent jet in that the mean velocity profiles approach self-similarity with increasing distance from the orifice (up to  $x/D_f = 9$ ). The jet responds like a compressible shear layer in that it spreads more slowly at higher Mach numbers (up to  $M_j = 0.7$ ) than at low Mach numbers. In contrast, the integral length scales and Kolmogorov constant of the turbulence are approximately invariant with respect to changes in either the Reynolds or Mach numbers. We briefly report on instrumentation under development that will extend the accessible Taylor-scale Reynolds and turbulent Mach numbers to 4000 and 0.3, respectively.

**Keywords** Compressible turbulence · Hot-wire anemometry · Free-stream turbulence

## 1 Introduction

Hydrodynamic fluctuations in compressible turbulence play a determining role in engineered and natural flows (Lele, 1994; Gatski and Bonnet, 2013). A relatively long history of controlled experimentation combined with theoretical analysis generates a detailed picture of incompressible turbulence (e.g. Pope, 2001; Davidson et al., 2012; Sinhuber et al., 2015), where the main parameter in the problem is the Reynolds number. Though this picture is far from complete, it is much clearer than the one we have of compressible turbulence, where we have in addition to this parameter the Mach number and others whose roles have yet to be established definitively (Danish et al., 2016; Donzis and John, 2019; Sabelnikov et al., 2021).

---

N. Manzano-Miura  
Cornell University, Sibley School of Mechanical and Aerospace Engineering, Ithaca, NY, USA  
E-mail: pnm24@cornell.edu

D. Gloutak  
University of Colorado Boulder, Ann and HJ Smead Aerospace Engineering Sciences, Boulder, CO, USA

G.P. Bewley  
Cornell University, Sibley School of Mechanical and Aerospace Engineering, Ithaca, NY, USA

In turbulence, fluctuations at small-scales depend sensitively on the Reynolds number in ways that can be difficult to distinguish from Mach number dependencies (Jagannathan and Donzis, 2016). For instance, intermittency measured by the flatness of velocity derivatives increases as a power law of the Reynolds number, and is likely dependent on the Mach number in a way that depends on the flow geometry at the small-scale (be it vortex-like or shock-like). Due to the increased mathematical complexity and the larger parameter space that the turbulence explores, there is less empirical or theoretical information available about compressible turbulence than about incompressible turbulence. For example, the energy dissipation rate, the small-scale structure of the flow, the shape of the energy spectrum, the translation between compressible forcing in simulations and realistic forcing in experiments, and the dependence of these features on the parameters in the problem are unknown.

Although the work on free shear flows has clarified the main mechanisms by which compressibility dampens turbulent mixing, recent computer simulations suggest profound changes in the structure of compressible turbulence relative to incompressible turbulence, such as a sign change in the skewness of the distribution of pressure fluctuations or a rapid increase in the dilatational dissipation rate with increasing Mach number (Jagannathan and Donzis, 2016). Moreover, recent literature discusses alternative mixing inhibition mechanisms that include the changing role of pressure and the influence of the orientation of disturbances at high Mach numbers (Karimi and Girimaji, 2016, 2017). Even at subsonic mean speeds, turbulent fluctuations can be fast enough relative to the speed of sound that regions of local compression and expansion appear in the flow, albeit less frequently than at higher speeds (Jagannathan and Donzis, 2016; Wang et al., 2018). The data needed to generate, validate and improve compressible turbulence models (Georgiadis et al., 2014; Quadros et al., 2016b) are scarce due to difficulties in generating compressible flows with negligible density gradients (unlike in Charonko and Prestridge (2017) where variable density effects are characterized) in which turbulent fluctuations can be fully resolved. In laboratory experiments the turbulent scales of motion are too small or too fast for most instrumentation. In contrast, in nature the conditions cannot be controlled.

The wide range of applications in which compressible turbulence appears suggests a broad utility for an understanding of its universal aspects. In hypersonic boundary layers, for instance, not only the mean flow but also the fluctuations are compressible (Owen et al., 1975; Spina et al., 1994; Williams et al., 2018). In scramjets and radial detonation engines combustion occurs at supersonic speeds, which translates to short residence times for the fuel and oxidizer in the combustor (Urzay, 2018; Ladeinde and Oh, 2021). In commercial and military aviation, the study of turbulence and its radiated sound have guided jet noise control strategies (e.g. Bodony and Lele, 2008; Jordan and Colonius, 2013). In astrophysical flows, star formation is slowed by supersonic turbulence (Low and Klessen, 2004; Federrath, 2013). The early Universe has been modeled as a turbulent fluid that experiences turbulent mass fluctuations over physical scales that extend to tens of megaparsecs (Shandarin and Zeldovich, 1989). These large-scale structures are associated with supersonic flows that generate cosmological shocks in the intergalactic medium (Ryu et al., 2008).

One of the few universal findings about compressible turbulent flows is that free shear layers grow more slowly at high Mach numbers than at low Mach numbers (Gatski and Bonnet, 2013). We briefly review these findings with a focus on turbulent jet experiments, since they resemble the experiments we performed. Schadow et al. (1990) reports Schlieren photography and total-pressure measurements and decreased spreading rates in coaxial jets at transonic Mach numbers ( $0.25 < M_c < 2.25$ , where  $M_c = (U_1 - U_2)/(c_1 - c_2)$  is the convective Mach number and the subscripts 1 and 2 denote the faster and slower streams), and a strong dependence on the practical definitions of the jet width and spreading rate. The convective Mach number was modulated in part by varying the density ratio between the center and coaxial jets. The density ratio, whose effects are not studied here, also alter the development of compressible jets. Samimy et al. (1993) finds that vortex generators at the jet orifice ( $0.3 < M_j < 1.81$ , where  $M_j = U_j/c$  is the jet Mach number and  $U_j$  is the jet speed at the orifice) increase jet spreading rates in a way that depends on geometry but not on Mach number. Zaman (1998, 1999) also finds different behaviors for different nozzle geometries as well as decreased spreading and centerline velocity decay rates for round jets ( $0.29 < M_j < 1.97$ ) above Mach one. Fleury et al. (2008) uses Particle Image Velocimetry (PIV) to find self-similar space-time correlations both off-axis and on-axis in subsonic isothermal round jets ( $0.6 < M_j < 0.9$ ), as well as smaller integral scales at higher Mach numbers. Feng and McGuirk (2016) studies subsonic but compressible annular shear layers in addition to supersonic ones, ( $0.2 < M_c < 0.6$ ) and states that their slower growth at higher Mach numbers starts at lower  $M_c$  than for planar mixing layers and is stronger at comparable  $M_c$ .

Numerical simulations add detail to the experimental observation that compressible shear layers grow more slowly than incompressible ones. For instance, Sarkar and Lakshmanan (1991) implement a closure model and find reduced compressible shear layer growth rates consistent with experiments. Blaisdell et al. (1993) performs simulations of decaying isotropic, homogeneously sheared turbulence, and also finds a reduced growth rate of turbulence attributed to an increase in the dissipation rate accompanied by an energy transfer to internal energy by the pressure-dilatation correlation. Freund et al. (2000) reports direct numerical simulations (DNS) of annular mixing layers ( $0.1 < M_c < 1.8$ ,  $0.2 < M_j < 3.5$ ,  $M_t$  up to 0.8), which resemble the early development of a round jet, and explains suppressed growth rates by the budget of the streamwise component of Reynolds stresses – whereas shear stresses and radial and azimuthal normal stresses are suppressed at high Mach numbers, the axial normal stresses stay the same, causing a shear stress anisotropy which decreases with Mach number. This latter study also identifies a decrease in transverse length scales due to an acoustic timescale limitation, which eventually causes large flow structures to deform faster than sound can propagate through them, disabling the formation of coherent eddies. Sandberg et al. (2012) reports DNS of a compressible jet ( $0.46 < M_j < 0.84$ ) generated by a fully-developed pipe flow exiting into a low Mach number coflow, and finds that the self-similarity of coflowing jets breaks down for coflow values larger than about 40% of the jet speed. Arun et al. (2019) reports a DNS of high-speed mixing layers ( $0.2 < M_c < 1.2$ ) and finds that with increasing  $M_c$ , an increase in vortex-dominated regions accompanies a reduction in shear layer growth rates.

These findings are generally consistent with the observation that mixing layers spread more slowly at higher Mach numbers, an observation embodied in the Langley curve (Slessor et al., 2000). Taken together, the results also suggest an important dependence on the conditions of the flow at any given Mach number, and that different geometries produce different behaviors. The way turbulence changes with increasing Mach number needs to be explained and the mechanisms at work need to be separated from those associated with changes in the Reynolds number and geometry. While the convective Mach number controls turbulent flow parameters such as the spreading rate of shear layers, turbulence properties such as the flatness of velocity derivatives (Tang et al., 2018) depend on the Reynolds number, for instance, as do the slope of the energy spectrum (Praturi and Girimaji, 2019), the intermittency exponent (Yakhot and Donzis, 2018), and the scaling exponents of structure functions (Iyer et al., 2020).

Incompressible turbulence within jets exhibits an approximate  $-5/3^{\text{rds}}$  power-law in energy spectra even in the near-field and at distances from the orifice smaller than those over which the jet is self-similar (Fellouah et al., 2009). This rapid development of the characteristic turbulence spectrum has also been observed in wakes and behind grids (Braza et al., 2006; Valente and Vassilicos, 2012). The spectrum may be steeper for compressible flows, when shocks are dominant for instance, and even for  $M_t$  as low as 0.1 (Bertoglio et al., 2001; Donzis and Jagannathan, 2013; Federrath, 2013; Wang et al., 2017, 2018). Such a steeper spectrum was reported in Biagioni and D’Agostino (1999) in a hypersonic wind tunnel flow albeit at an axial distance less than one nozzle diameter, where a  $-11/3^{\text{rds}}$  power law was in agreement with the compressible spectrum predicted by an Eddy Damped Quasi-Normal Markovian (EDQNM) model but inconsistent with a cascading picture characteristic of fully developed turbulence.

This paper reports the first local quantitative measurements in compressible turbulence in the Variable Density and Speed of Sound Vessel (VDSSV), along with details of its design principles and capabilities. We describe the turbulent jet flow produced within our facility and its evolution with Mach number to benchmark the conditions in which the turbulence develops. We generate a compressible flow and report quantities including two-point correlations, turbulent Mach number profiles, Kolmogorov constants, spectra, and their evolution with Mach number. We then compare our results with previous work.

## 2 Apparatus and Methods

To raise the Mach number at constant Reynolds number and for fixed boundary conditions, we compared experiments performed in air with ones performed in  $\text{SF}_6$ . The chief advantage of  $\text{SF}_6$  is that its speed of sound is approximately 2.5 times lower than the one for air. In contrast to air-breathing facilities running at similar Reynolds and Mach numbers,  $\text{SF}_6$  experiments operate at lower speeds that are easier to resolve temporally since timescales are set by the speed of sound at any given Mach number. Similarly, the small scales of turbulence are larger and slower at a given Mach number which enables improved spatial resolution. Additionally,  $\text{SF}_6$  experiments generate lower forces that ease mechanical

**Table 1:** Gas properties.  $P$  is the static pressure,  $\mu$  is the dynamic viscosity,  $\gamma$  is the specific heat ratio,  $c$  is the speed of sound,  $T$  is the mean gas temperature,  $\rho$  is the mean gas density.

Gas	$P$ [bar]	$\mu _{1bar}$ [Pa · s]	$c$ [m/s]	$\rho$ [kg/m <sup>3</sup> ]	$T$ [K]
Air	1.0	$1.845 \times 10^{-5}$	345	1.17	300
SF <sub>6</sub>	0.165	$1.549 \times 10^{-5}$	136	0.97	300

design, consume less power and so facilitate electrical design, and can be run continuously in contrast to blow-down or burst-disk experiments so that statistics better converge. Finally, measurements from high (SF<sub>6</sub>) and low (air) Mach number experiments can be made with the same probes operating at the same frequencies.

An alternate strategy of raising the Mach number of a gas flow at constant Reynolds number and fixed geometry is to increase the flow speed while simultaneously decreasing the pressure at constant temperature. This is so since the Reynolds number is proportional to changes in the gas density, while the speed of sound and dynamic viscosity are insensitive to it. This strategy was employed in the 1950's in the Variable Density High Speed Cascade Wind Tunnel at the Deutsche Forschungsanstalt, in which the gas pressure was varied between 0.1 and 1 bar and the mean flow Mach number between 0.2 and 1.1 in order to characterize the performance of compressor blade cascades (Schlichting, 1956). This strategy, however, comes at the cost of increasing the frequency of the fluctuations that need to be detected (in proportion to the Mach number), so that faster instruments are needed at higher Mach numbers. To compare high and low Mach number measurements of turbulent fluctuations therefore, the frequency response of the instruments needs to be understood (Hutchins et al., 2015). Even with the improvements in measurement technology since Schlichting (1956), we need to bring down the speed of the flow while holding constant its Mach number.

## 2.1 Pressure vessel

We conducted experiments in a 16 bar pressure vessel (Fig. 1 and Fig. 2) consisting of two 0.6 m long cylindrical sections with 1 m diameter and two rounded end caps made of hot-rolled steel. Each half of the vessel is mounted onto a cart that rolls on rails in order to pull the halves apart and to open the full cross section of the vessel to the experimenter. The length of the pressure vessel, now 1.7 m, can be extended to 3 m with the addition of annular sections between the two halves. Acrylic windows bolted to 30 cm diameter portholes welded onto the shell provide optical access up to gas pressures of about 3 bar (Gloutak, 2018). These acrylic windows can be exchanged with smaller sapphire windows (not shown) to extend this access up to 16 bar.

To run experiments with SF<sub>6</sub>, the VDSSV was first evacuated with a vacuum pump down to an absolute pressure of 0.01 bar after ensuring that no leaks were present per Rottländer et al. (2016), keeping the leak rate below  $1.6 \times 10^{-1}$  mbar L/s. The facility was then charged to a set pressure from an external tank using a system of pumps and compressors (Enervac's GRU-4 SF<sub>6</sub> Recovery Unit). After each experiment, the gas was stored and recycled. At a pressure of 0.165 bar, the density of SF<sub>6</sub> is such that the kinematic viscosity,  $\nu = \mu/\rho$ , is the same as the one for air, and consequently the Reynolds numbers are matched.

## 2.2 Turbulence generation

A 12-blade ducted fan with a diameter  $D_f = 90$  mm produced a turbulent jet which expanded down the centerline of the pressure vessel (see Fig. 2). In this sealed environment, the jet discharge fluid and the entrained external ambient fluid were identical. The fan drew up to 2.4 kW of electrical power, part of which was converted into mechanical energy in the flow, and all of which was ultimately converted into heat. Fan exit flow velocities, measured by a Pitot tube, ranged from 10 to 90 m/s, corresponding to jet Mach numbers up to approximately 0.7. This is well into the compressible regime, which is conventionally taken to prevail when  $M_j > 0.3$ . When the turbulent jet impinges on the pressure vessel wall opposite to that of the fan, it generates a return flow near the outer walls of the pressure vessel (Fig. 2), as in other turbulent jet experiments in enclosed facilities (e.g. Chanal et al., 2000). The return flow is slower than the jet

by a factor of about one hundred, which is the ratio of cross-sectional areas between the jet and the annulus around it, and is always subsonic. From the mean rotation rate of a streamer in the jet, we estimated that the swirl number,  $S = U_\theta/U_j$ , which compares the the azimuthal to axial components of momentum, was smaller than 0.08 over the full range of fan speeds. Swirl tends to increase jet spreading rates when it is larger than 0.6 (Gilchrist and Naughton, 2005; Vanierschot and Van den Bulck, 2008), which is the opposite of the expected effect of compressibility.

We classified our observations in terms of the Taylor microscale Reynolds number,  $R_\lambda = u'\lambda/\nu$  and the turbulent Mach number,  $M_t = \sqrt{3}u'/c$  (Samtaney et al., 2001). The factor of  $3^{1/2}$  has its origin in the isotropic assumption that  $u' \approx v' \approx w'$ , which we retain though jet turbulence is anisotropic, particularly at its margins. As shown below, the jet comprises velocity fluctuations up to approximately  $u' = 15\text{ m/s}$ , corresponding to  $R_\lambda$  up to 2000 and  $M_t$  up to 0.2.

### 2.3 Diagnostic apparatus

We used constant temperature anemometry (CTA) with hot-wire probes that resolved inertial-range statistics. The VDSSV produces a subsonic, compressible jet whose Kolmogorov scales can be as small as 10 microns. The probes were made of Wollaston wire, and measured 0.6 microns in diameter and about 120 microns in length, which corresponds to a spatial resolution of between 1 and 12 Kolmogorov scales. Hot wires measure a cooling rate due to heat transfer rate from the wire to the flow, which in this paper we interpret as a cooling velocity,  $u$ . In the compressible flow regime, hot wires respond to both mass flux and temperature fluctuations. The balance between these two types of fluctuations depends on the Mach number (Quadros et al., 2016a) and on the wire temperature. In the present experiment, the probes were operated at an overheat ratio of 1.4, so that the probes responded predominantly to mass flux fluctuations. Assuming that the Strong Reynolds Analogy holds (Gatski and Bonnet, 2013), density fluctuations were approximately 0.04 % of the mean at an axial position of 9 fan diameters, where turbulence measurements are reported. Hence, density fluctuations were considered small enough compared to the velocity fluctuations, which at the jet center achieved values of 25 % of the mean.

Resolving diminutive scales is challenging not only due to the limited spatial resolution of modern probes, but also due to the proximity to the limit between the continuum regime and the slip-flow regime. Measurements in this regime were performed, for instance, by Kokmanian et al. (2019), where a modified version of the state-of-the-art nanoscale thermal anemometry probes (NSTAPs) were used to measure turbulence at supersonic conditions, and found a linear relationship between Reynolds number and Nusselt number due to the closeness of the probe diameter to the mean free path of molecules (Knudsen number,  $Kn \sim O(1)$ ). In our experiment, the mean free path in  $\text{SF}_6$  is approximately 200 nm, corresponding to a wire-diameter based Knudsen number of 0.33, and a micro-structure Knudsen number, based on the Kolmogorov scale, of 0.017. The former Knudsen indicates that our probes are not strictly operating on a continuum flow regime. The latter Knudsen number suggests that, at low speeds of sound, the smallest flow scales produced in the experiment are marginally within the continuum limit. In fact, the micro-structure Knudsen number increases linearly with  $M_t$  and with the inverse square root of  $R_\lambda$  (Gatski and Bonnet, 2013). Hence, in the limit of very low Reynolds numbers and very high Mach numbers, turbulent eddies may interfere with molecular motion (Tennekes and Lumley, 2018). Nevertheless, we discard this possibility in our experiment, as it produces Reynolds numbers high enough to enable experimentation for a broad range of Mach numbers where the motion of gas molecules is in statistical equilibrium and molecular transport effects can be represented by transport coefficients such as the viscosity.

Hot-wire voltages were acquired at streamwise positions between  $x/D_f = 1.9$  and 9.1, which we call station 1 and station 2, and sampled with a digital acquisition card (16-bit NI-USB 6221) at a frequency,  $f_s$ , of 200 kHz for approximately 10 s (corresponding to about  $1.7 \times 10^4$  to  $1.7 \times 10^5$  integral time scales), and low-pass filtered at the Nyquist frequency,  $f_{Nyq}$ , of 100 kHz to prevent aliasing.

The probes were calibrated *in situ* against a Pitot tube while varying the fan speed. We employed King's Law to relate mean voltages and speeds (King, 1914), along with a temperature correction (Bruun, 1996). Along the axis of a jet, the velocity distribution is approximately Gaussian (Anselmet et al., 1984). Chanal et al. (2000) exploit this fact to determine a calibration from the differences between a measured hot-wire voltage distribution and a Gaussian

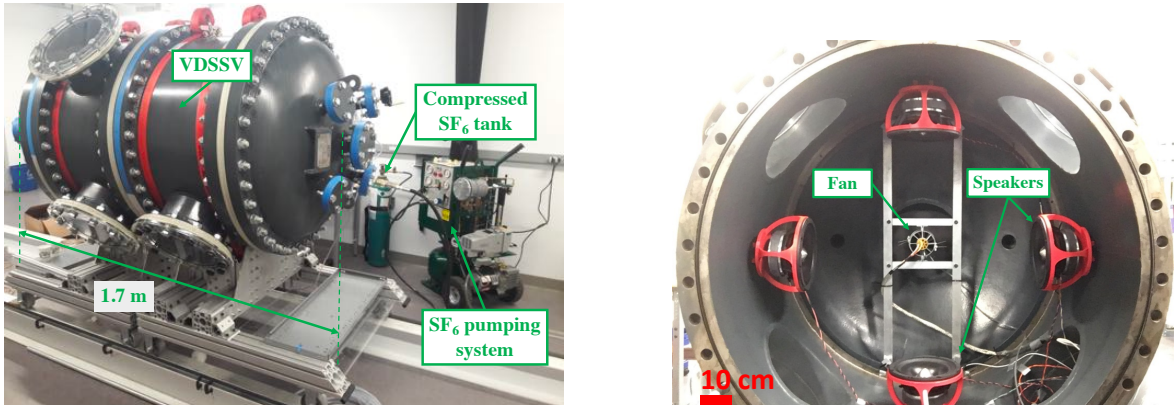


**Fig. 1** *Top*: The facility includes the VDSSV, a compressed SF<sub>6</sub> storage tank, and the SF<sub>6</sub> gas-handling system. Windows provide optical access through five 30 cm portholes. The VDSSV is mounted on carts and rails, so that its two halves can be separated to access its interior. *Bottom*: A view upstream along the axis of the VDSSV, once it has been separated along its midline, shows the fan that produces the turbulence characterized in this paper. The red cages house loudspeakers for acoustic experiments not discussed here.

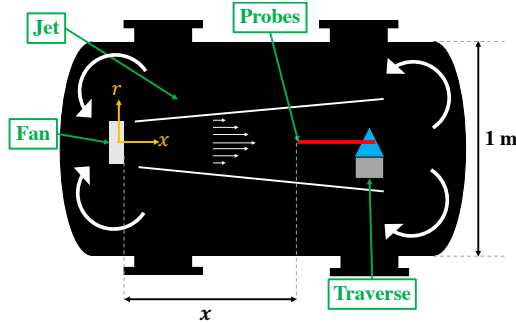


**Fig. 2** A sketch (not to scale) of the interior of the VDSSV shows the configuration of the fan and probes. The distance between the fan and the wall upstream of it is 25 cm. The distance along the axis of the fan from its outlet to the probe ( $x$ ), can be varied between 0.1 and 1.3 m (1 and 15 fan diameters). Orthogonal to the  $x$ -direction,  $r$  is the radial distance outward from the centerline.

distribution modified to account for probe behavior at near-zero speeds, such that

$$P(u) \propto u^2 \exp\left(-\frac{(u-U)^2}{2\sigma^2}\right) \quad (1)$$

where  $u(x, t)$  is the flow speed,  $U = \langle u \rangle$  is its mean, and  $\sigma^2 = \langle u^2 \rangle$  is its variance. We used this method to extend the calibration given by King's law to velocities beyond those for which we made Pitot tube measurements. The spatial structure of turbulence was investigated by invoking Taylor's Hypothesis of frozen turbulence (Taylor, 1937). We estimated the turbulent kinetic energy dissipation rate,  $\epsilon$ , from the inertial-range scaling of second-order velocity structure functions, particularly by taking the plateau value in  $S_2 = C_2(\epsilon r)^{2/3}$  and solving for  $\epsilon$  (Pearson et al., 2002). Large scale turbulence statistics were computed as follows. The amplitude of velocity fluctuations was  $u' = \langle u^2 \rangle^{1/2}$ . The integral scale was taken as the area under the velocity autocorrelation function,  $L = \int_0^\infty f(r) dr$  with  $f(r) = \langle u(x+r)u(x) \rangle / \langle u^2 \rangle$ , where the tails for correlations below 0.1 were calculated from integrals of exponential fits to the autocorrelation functions between values of  $1/e$  and 0.1 (Bewley et al., 2012). The Taylor microscale was computed as  $\lambda = u' \sqrt{15\nu/\epsilon}$ , and the Kolmogorov length scale as  $\eta = (\nu^3/\epsilon)^{1/4}$ .

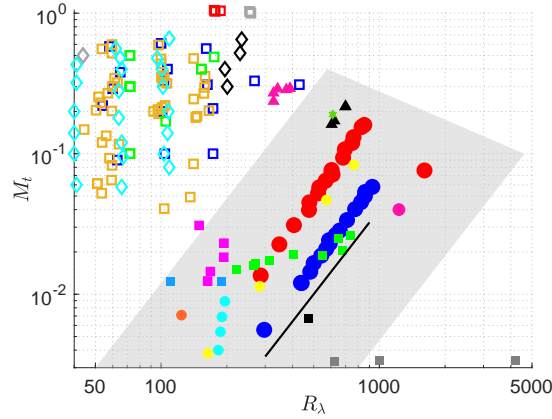


**Fig. 3** The  $R_\lambda - M_t$  parameter space achieved in various experiments (closed symbols) and simulations (open symbols). Different shapes correspond to different flow type as follows: jets (circles), boundary layers (hexagrams), mixing layers (triangles), homogeneous shear (diamonds), and homogeneous isotropic flows (squares). Our data are shown as closed blue and red circles for air and SF<sub>6</sub>, respectively. Other sources of experimental data are as follows. Circles: light blue (Wyganski and Fiedler, 1969), orange (Hussein et al., 1994), magenta (Biagioni and D’Agostino, 1999), yellow (Narayanan et al., 2002). Hexagrams: green (Spina and Smits, 1987). Triangles: magenta (Barre et al., 1994), dark gray (Bowersox and Schetz, 1994). Squares: black (Mydlarski and Warhaft, 1996), light blue (Zwart et al., 1997), magenta (Honkan and Andreopoulos, 1992), light green (Briassulis et al., 2001), gray (Bodenschatz et al., 2014). An abundance of approximately incompressible turbulence experiments not shown lie below  $M_t = 0.01$  (e.g. Sinhuber et al., 2015). The DNS are as follows. Squares: green (Samtaney et al., 2001), red (Wang et al., 2011), gray (Wang et al., 2012), dark blue (Donzis and Jagannathan, 2013), orange (Donzis and John, 2019). Diamonds: gray (Blaisdell et al., 1993), light blue (Chen et al., 2018), black (Wang et al., 2018).

### 3 Results

We survey mean flow characteristics as well as turbulence statistics in the turbulent jet and compare the data with those available in the literature. A description of the parameter space covered by the present experiment is followed by a characterization of the turbulent jet at stations 1 ( $\approx 2D$ ) and 2 ( $\approx 9D$ ), and their evolution with increasing Mach number, all of which anchor our analysis of second-order turbulence statistics such as autocorrelation functions and spectra.

### 3.1 Parameter Space

The parameter space of the Reynolds number ( $R_\lambda$ ) and turbulent Mach number ( $M_t$ ) accessed in a representative collection of experiments and numerical simulations drawn from the literature is shown in Fig. 3. Data from simulations, most of which are DNS, span a range of turbulent Mach numbers up to approximately 1.0 and Taylor Reynolds numbers rarely exceeding 100. At higher Reynolds numbers, the simulation of compressible turbulence becomes prohibitive in terms of computational cost and the small-scale flow physics need to be modeled. Additionally, low Mach number simulations are difficult due to the separation of the acoustic and turbulence time scales.

Previous experiments, in contrast to simulations, easily reach Reynolds numbers  $R_\lambda > 100$ , a regime in which turbulence is well developed in the sense that an inertial subrange emerges where turbulence is only weakly affected by boundaries and friction (Pope, 2001). Attaining high Mach numbers in experiments poses challenges both from the power requirement and measurement resolution perspectives. Turbulent Mach numbers in excess of 0.2 are reached in some boundary layer experiments (e.g. Spina and Smits, 1987), where the mean flows are typically too fast to enable high resolution measurements.

Our experiments in the VDSSV (gray trapezoid) bridge a sparsely populated space between previous experiments that tend to occupy the low Mach number, high Reynolds number region, whereas numerical simulations reside in the high  $M_t$ , low  $R_\lambda$  region. To the left and right, the space is bounded by the lowest (0.05 bar) and highest (15 bar) gas pressures in the VDSSV. To the top right, the space is bounded by the power of the fan, where  $M_t \sim R_\lambda^{-1}$  since the maximum power of the fan is  $P_{max} \sim R_\lambda^2 M_t^2$ , which assumes  $P_{max} \sim \rho U_j^3$  and  $u \sim U_j$ . In the VDSSV,  $M_t$  and  $R_\lambda$  can be adjusted independently by changing between working gases that have different sound speeds, and by adjusting mean jet velocities (moving up and down along the blue and red curves). Two representative trajectories followed by our experiments for 1 bar air and 0.165 bar SF<sub>6</sub> show that the Mach number grows approximately as the square of the Reynolds number (black line:  $M_t \sim R_\lambda^2$ ) while increasing the fan speed and holding all else constant. This quadratic scaling holds if the flow velocity changes while its length scales do not, since  $M_t \sim u'$  and  $R_\lambda \sim u'^{1/2}$ .

### 3.2 Jet profile characteristics

The jet at its center is shear free and exhibits velocity fluctuations up to 15 m/s. Velocity measurements at station 1 were performed to assess the flow structure of the jet in its initial development. Turbulence measurements were performed in the developed region of the jet and past a wake region that extends to approximately  $x/D_f = 5$ , where shear layers emanating from the fan become well-mixed with the wake and form a jet with an approximately self-similar profile.

#### 3.2.1 Similarity at station 1

At  $x/D_f = 1.9$ , near the fan outlet, the mean velocity profiles were approximately invariant with respect to changes in the Mach number (Fig. 4). The profiles were measured at six representative pairs of jet Mach numbers ranging from  $M_j = 0.04$  to 0.72, with each pair at a constant Reynolds number. There is a velocity deficit in the central part of the jet out to  $0.5R_f$  from the centerline, which corresponds to a wake whose width is approximately the same as the fan motor diameter. Normalization of radial positions by the fan radius collapses all of the data out to at least  $r/R_f \approx 1$ , consistent with the width being determined by the size of the orifice near the outlet. At larger radial distances, the seemingly higher velocities outside of the jet core at the two lowest  $M_j$  are a result of a bias in the measurement due to two reasons. First, since the hot-wire measurements are unsigned, the resulting error is positive and thus cumulative. Second, in addition to random error we have systematic errors due to deviations of the calibration curve detailed in Section 2.3 from King's Law at very low speeds. Error bars at the highest and lowest  $M_j$  indicate that the differences between the speeds at the tails are statistically insignificant. The inset shows the jet centerline velocity, normalized by the jet exit velocity, as a function of jet Reynolds number, which approaches a constant value of approximately 0.8, a lower value compared to a compressible jet in Narayanan et al. (2002) due to the influence of the wake.



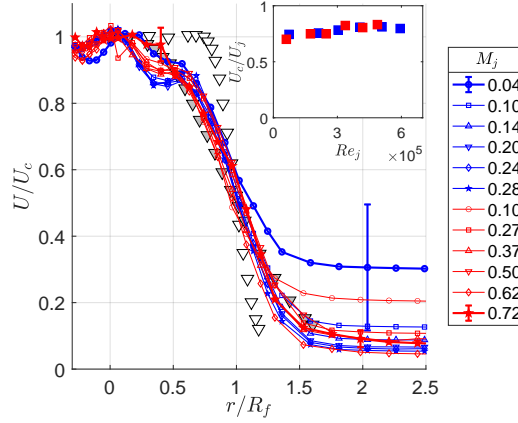


**Fig. 4** Radial mean velocity profiles close to the outlet of the fan ( $x/D_f = 1.9$ ) normalized by the centerline mean velocity ( $U_c$ ) in air (blue) and SF<sub>6</sub> (red) are approximately invariant with respect to changes in Mach number. The radius of the fan is  $R_f = D_f/2 = 45$  mm. At large  $r$  the differences between the measured profiles and zero are not significant since the uncertainty is large at small velocities. Data from Narayanan et al. (2002) at  $M_j = 0.6$  (triangles, open and closed symbols at  $x/D_f = 1$  and 4, respectively) are shown for reference, for which  $R_f$  is the half-width of the jet ( $R_{1/2}$ ) and not the radius of the jet orifice. *Inset:* Centerline mean velocity,  $U_c/U_j$ , as a function of jet Reynolds number,  $Re_j = U_j D_f / \nu$ .

Data from Narayanan et al. (2002) at  $M_j = 0.6$  are shown for comparison with our data, which displays a top-hat profile characteristic of near-orifice jet profiles at  $x/D = 1$  that quickly decays toward a rounded shape at  $x/D = 4$ . The profiles in our experiment at two diameters are bounded by the data from Narayanan et al. (2002) for  $r/R_f > 0.5$ , but presents flow irregularities at smaller radial distances due to the influence of the fan geometry.

### 3.2.2 Similarity at station 2

At 9.1 diameters from the fan (Fig. 5) the data collapse with each other when radial positions are normalized by the half-width radii of the jets ( $R_{1/2}$ ). The profiles align with those from Narayanan et al. (2002) at similar Mach numbers and distances from the orifice ( $M_j = 0.6$  and  $x/D = 6$  and 10), and are indistinguishable from the normalized profiles of an incompressible jet at 98 diameters from the orifice (not shown) in Wygnanski and Fiedler (1969). These results suggest an approximate self-similarity of the jet.

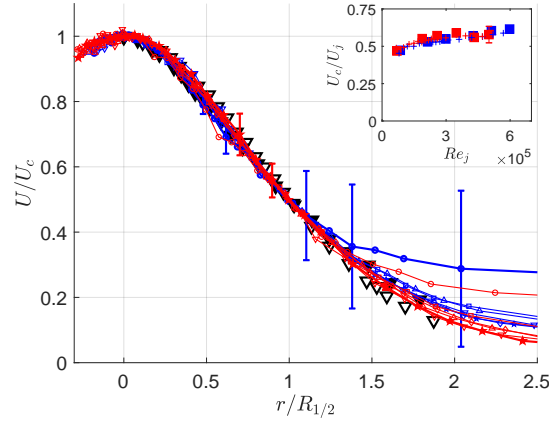


**Fig. 5** The profiles collapse when scaled by their half-widths,  $R_{1/2}$ . Data from Narayanan et al. (2002) at  $M_j = 0.6$  (black triangles) are shown for reference, with open and closed symbols corresponding to streamwise positions  $x/D_f = 6$  and 10 respectively. The error bars represent uncertainty in the calibration of the hot wire, which is largest at low speeds and far from the jet axis. Different markers correspond to Mach numbers as in the legend for Fig. 4. *Inset:* Jet centerline speed,  $U_c/U_j$ , variation with jet Mach number with error bars representing uncertainty in calibration (many of them smaller than the symbols).

### 3.2.3 Jet width development

At low Mach numbers, the jet spreads such that its diameter is at least one-third larger at 9 diameters downstream than at 2 diameters downstream (Fig. 6, top). As the Mach number increases, the width of the jet at station 2 (circles) narrows and approaches the jet width at station 1 (triangles), and so the width of the orifice itself. In other words, the jet approaches a “turbulent laser” that does not diverge with increasing distance from its source at high Mach numbers. Axial momentum transport may be inhibited in the radial direction at higher Mach numbers by mechanisms including smaller transverse velocity fluctuations, which are not measured here (Arun et al., 2019; Matsuno and Lele, 2021).

We characterize the jet spreading rate by  $\alpha \equiv \Delta R/\Delta x$ , which is the difference between up- and down-stream diameters,  $\Delta R = (R_{1/2}(x/D_f = 9.1) - R_{1/2}(x/D_f = 1.9))$ , divided by the distance between the up- and down-stream positions,  $\Delta x$ . We make the spreading rate relative to the median of the ones for which  $M_j < 0.2$ , which is  $\alpha_0$ , and we assumed a constant virtual origin with increasing Reynolds number. The virtual origin is insensitive to the Reynolds number, but depends strongly on inflow conditions and strength of disturbances (Pitts, 1991; Boersma et al., 1998). Normalized jet growth rates decrease with jet Mach number (Fig. 6, bottom). This trend is qualitatively consistent with and analogous to the Langley curve (black dashed line), where a 40% decrease in normalized compressible shear layer growth rate can

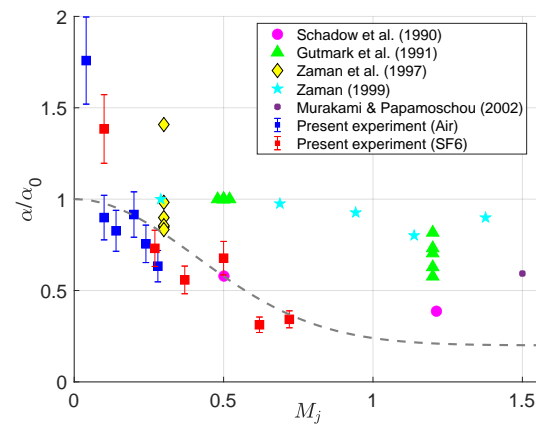
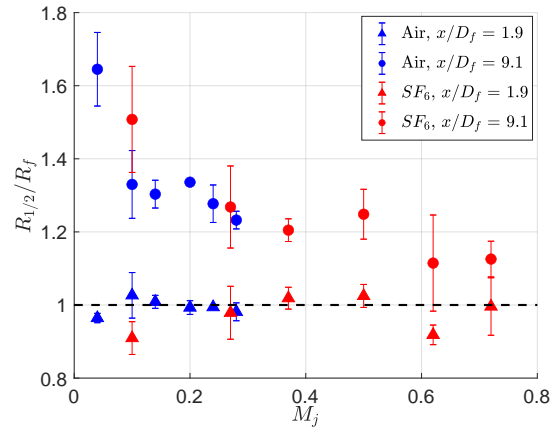


**Fig. 6** *Top*: Jet widths at  $x/D_f = 9.1$  (circles) decrease with increasing Mach number, while at station 1 (triangles) the width does not change. The error bars are the differences between two experiments performed under the same conditions. *Bottom*: We interpret the difference between down- and up-stream jet widths as a spreading rate,  $\alpha$ . This spreading rate decreases with increasing jet Mach number,  $M_j$ . The data are qualitatively consistent with a Langley-like curve, embodied in a fit (dashed black line) of the form  $a + (1 - a) \exp(-bM_j^2)$  where  $a$  and  $b$  are equal to  $1/5$  and  $3/2$ , respectively.

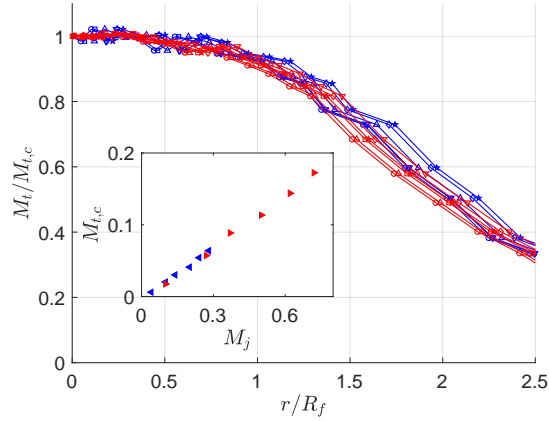


**Fig. 7** From the centerline out to about one fan radius ( $r/R_f = 1$ ), the turbulent Mach number ( $M_t$ ) is approximately homogeneous in air (blue) and SF<sub>6</sub> (red) at  $x/D_f = 9.1$ . *Inset:* The turbulence Mach number on the centerline,  $M_{t,c}$ , increases linearly with the jet Mach number,  $M_j$ . Markers correspond to Mach numbers as in the legend for Fig. 4.

be observed at a jet Mach number as low as 0.5. Our data is compared to previous jet studies that measured spreading rates in the range of axial positions of  $2 < x/D < 30$  (Schadow et al., 1990; Gutmark et al., 1991) or  $2 < x/D < 20$  (Zaman et al., 1997; Zaman, 1999; Murakami and Papamoschou, 2002), which overlaps with the distances over which spreading rates were characterized in the present experiment. The apparent initial increase in spreading rate is due to a high uncertainty on the fringes of the jet at the lowest  $M_j$ . Unlike the relatively good collapse in the mixing layer study by Barone et al. (2006), the variability in the jet data for any given Mach number is an indication of sensitivity to initial and boundary conditions, and therefore of non-universality in terms of the Mach number, in addition to measurement uncertainties and differences in practical definitions of the spreading rate between experiments.

### 3.3 Turbulence at station 2

Here we examine the outer scales of the turbulence at station 2, located at the furthest distance from the orifice at which we measured in the present experiments ( $x/D_f = 9$ ).

#### 3.3.1 Homogeneity

At station 2 ( $x/D_f = 9.1$ ), the turbulence in the jet is approximately homogeneous within one jet diameter, in the sense that the turbulent Mach number is constant to within about 5% up to one fan radius for all conditions (Fig. 7).

It is interesting that the turbulent Mach number profiles do not narrow as quickly with Mach number as the mean profiles, so that the turbulence intensity,  $u'/U$ , grows to larger values at the fringes of the jet at higher Mach numbers. The inset shows that the turbulent Mach number at the center of the jet increases linearly with the jet Mach number, attaining a maximum value of  $M_t = 0.17$  when  $M_j \approx 0.7$ . On the center-line, the turbulence intensity at station 2 was between 20% and 24% of the mean velocity. This compares with upstream intensities between 8% and 14% at  $x/D_f = 1.9$  and on the center-line.

### 3.3.2 Autocorrelations and integral scales

Along the centerline and at station 2, the longitudinal velocity correlation functions,  $f$ , collapse approximately when rescaled by the correlation lengths,  $L$ , defined in Sec. 2.3 (Fig. 8, top). These correlation lengths,  $L$ , are themselves approximately independent of the Mach number (Fig. 8, bottom). Despite the strong fluctuations, we interpret the correlations as spatial functions of  $\Delta x = U\Delta t$ , according to Taylor's Hypothesis (Lee et al., 1992), where  $\Delta t$  is the time interval between velocity measurements, though this interpretation is not necessary here.

A small but systematic trend in the correlation functions is magnified by making the difference between the high (SF<sub>6</sub>) and low (air) Mach number correlation functions at each Reynolds number (Fig. 8, inset). When the Mach number is raised at constant Reynolds number, slightly faster decorrelations are introduced at separations smaller than the integral length scale, as quantified by the magnitude of the first troughs in the inset, and are compensated by stronger correlations at large separations. This effect is more prominent with increasing Reynolds number (indicated by the colorbar).

In incompressible turbulence, integral scales depend weakly on the Reynolds number. The dependence on Mach number, however, is not entirely clear. At  $x/D_f = 9.1$  and the jet center, integral scales normalized by the fan diameter  $D_f$  remain relatively constant with jet Mach number at about  $0.45D_f$ , closely following the fan radius (Fig. 8, bottom). This aligns with the notion that integral scales are geometrically related to the scales of turbulence energy injection (White et al., 2002). Integral scales are slightly larger at the jet margins ( $r = R_f$ ) than at the jet center, achieving values slightly in excess of the fan radius on average.

### 3.3.3 Energy spectra

We observe that all spectra display a  $-5/3^{\text{rds}}$  scaling region consistent with incompressible dynamics up to the highest turbulent Mach number we reached,  $M_t = 0.17$  (Fig. 9). The observed inertial subrange extends over one to two decades for all flow conditions, indicating well-developed turbulence. At increasing flow speeds, our probes spatially truncated the smallest scales and did not capture them at the highest  $R_\lambda$  and  $M_t$ . At large wavenumbers, the cutoff in the spectra are determined by filters and not by the dissipation for all but the lowest Reynolds number data. The corresponding Kolmogorov scales range from  $20 \mu\text{m}$  to  $100 \mu\text{m}$  or between 400 and 2000 integral scales ( $L$ ). The inset shows that the Kolmogorov constant,  $C_\kappa$ , is independent of  $M_t$ .  $C_\kappa$  was estimated assuming isotropy, a  $-5/3^{\text{rds}}$  scaling between  $kL = 2$  and 20, and a constant value of one for  $C_\epsilon = \epsilon L/u'^3$ . Since we did not independently measure the dissipation, it is the trend, and not the particular value of  $C_\kappa$ , to which we draw attention.

## 4 Summary and conclusion

We detail the main design principles and capabilities of the VDSSV, a new facility that generates high-speed, subsonic compressible turbulent flows. Using hot-wire anemometry capable of resolving inertial subrange statistics, we report the first quantitative measurements in locally isotropic compressible turbulence. We highlight the VDSSV's unique ability to raise the Mach number at constant Reynolds number by switching the gas composition, while also attaining the highest turbulent Mach number,  $M_t = 0.17$ , in a free shear flow and in a controlled laboratory setting, to the best of our knowledge. We quantify turbulence at high Mach numbers at flow speeds low enough to enable high resolution measurements. Compressible flows in the pressure vessel were produced by means of a jet whose outlet is turbulent in SF<sub>6</sub>. The jet's spatial development showed that downstream mean profiles were approximately self-similar, while also

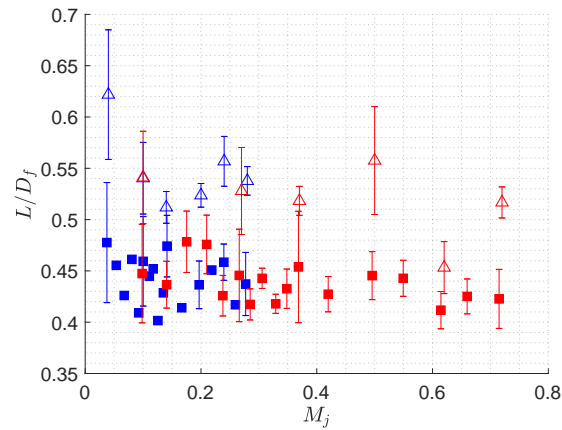
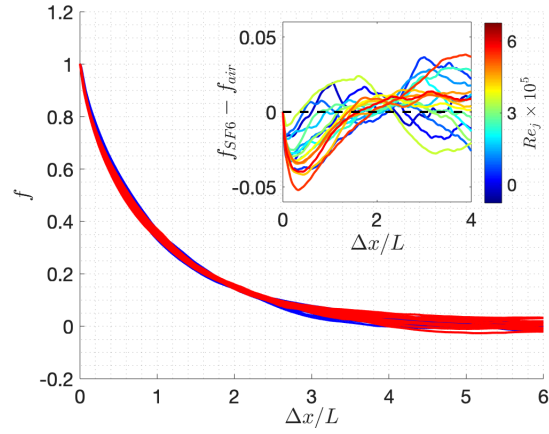


**Fig. 8** *Top:* The velocity correlation functions along the centerline at  $x/D_f = 9.1$  are approximately self-similar with respect to changes in Reynolds and Mach numbers, with a small systematic variation shown in the inset. The data are plotted as a function of separation,  $\Delta x$ , normalized by their integral time scales,  $L$ . *Inset:* The differences between pairs of correlation functions measured in  $\text{SF}_6$  and air at approximately the same Reynolds number, where the Reynolds number increases from blue to red curves. *Bottom:* The integral length scale,  $L$ , in fan diameters,  $D_f$ , is approximately independent of the Mach number on the center-line (closed symbols). Length scales at the margin of the jet (open symbols) are about 20% larger than those on the center-line. The error bars represent variation between different definitions of  $L$ , including  $L_e$ , which is the distance at which the autocorrelation function is equal to  $1/e$ .

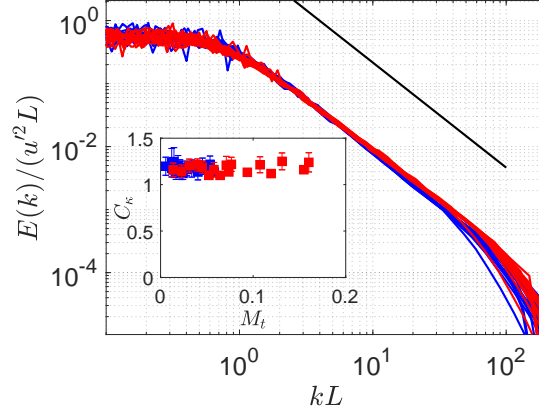


**Fig. 9** Energy spectra in air (blue) and SF<sub>6</sub> (red) collapse at small wavenumbers,  $k$ , under normalization by  $u'$  and  $L$ . The solid black line is a  $-5/3^{\text{rds}}$  power law. *Inset:* The Kolmogorov constant,  $C_\kappa$ , for these spectra is approximately independent of the Mach number,  $M_t$ .

spreading at slower rates at high Mach numbers. The pressure vessel can easily be extended to access larger  $x/D_f$  with the addition of cylindrical sections to its middle. Other upgrades may include the addition of heaters to generate a hot jet discharging into a colder environment. The streamwise turbulence in the jet was homogeneous in the radial direction within 5% up to one jet radius. Autocorrelation differences at a constant Reynolds but different Mach number revealed that initially faster decorrelations in the high Mach number cases are compensated by stronger correlations at large distances. Further experimentation is required to establish a clear link between these decorrelations and compressible or acoustic motions. Spectra and their Kolmogorov constants were unchanged by increases in the Mach number. Future experiments will aim to further characterize the jet at a broader range of streamwise positions, to provide more accurate estimates for the growth rates, and to quantify the recirculation on the sides of the jet. These experiments are projected to reach turbulent Mach numbers as high as 0.4 with the use of active grids (Griffin et al., 2019) and will additionally use optical instruments to track particles (Kearney and Bewley, 2020) and to measure density fluctuations.

**Acknowledgements** The authors are grateful to N. Dam and W. van de Water for the pressure vessel and for assistance from D. Donzis, L. Mydlarski and M. Ulinski. The authors also thank J. John, E. Liu, and H. Rivera for helpful discussions, a team of Master's students including E. Bair, A. Berberian, D. Cohen, D. Feng, T. Green, B. Oster, and K. Rajskey for designing, manufacturing and testing elements of the facility, and a team of undergraduates including Y. Atiq, S. Bell, W. Chan, M. Chen, S. DePue, C. Kartawira, A. Ramos Figueroa, K. Roberts, and C. Vahn for their help with data collection and experimental setup.

## References

- Anselmet F, Gagne Y, Hopfinger E, Antonia R (1984) High-order velocity structure functions in turbulent shear flows. *Journal of Fluid Mechanics* 140:63–89, DOI 10.1017/S0022112084000513
- Arun S, Sameen A, Srinivasan B, Girimaji S (2019) Topology-based characterization of compressibility effects in mixing layers. *Journal of Fluid Mechanics* pp 38–75, DOI 10.1017/jfm.2019.434
- Barone M, Oberkampf W, Blottner F (2006) Validation case study: prediction of compressible turbulent mixing layer growth rate. *AIAA journal* 44(7):1488–1497
- Barre S, Quine C, Dussauge J (1994) Compressibility effects on the structure of supersonic mixing layers: Experimental results. *Journal of Fluid Mechanics* 259:47–78, DOI 10.1017/S0022112094000030
- Bertoglio J, Bataille F, Marion J (2001) Two-point closures for weakly compressible turbulence. *Physics of Fluids* 13(1):290–310, DOI 10.1063/1.1324005
- Bewley G, Chang K, Bodenschatz E (2012) On integral length scales in anisotropic turbulence. *Physics of Fluids* 24(6), DOI 10.1063/1.4726077
- Biagioni L, D’Agostino L (1999) Measurement of energy spectra in weakly compressible turbulence. *AIAA 30th Fluid Dynamics Conference* DOI 10.2514/6.1999-3516
- Blaisdell G, Mansour N, Reynolds W (1993) Compressibility effects on the growth and structure of homogeneous turbulent shear flow. *Journal of Fluid Mechanics* 256(6):443–485, DOI 10.1017/S0022112093002848
- Bodenschatz E, Bewley G, Nobach H, Sinhuber M, Xu H (2014) Variable density turbulence tunnel facility. *Review of Scientific Instruments* 85(9), DOI 10.1063/1.4896138, 1401.4970
- Bodony D, Lele S (2008) Current status of jet noise predictions using large-eddy simulation. *AIAA journal* 46(2):364–380
- Boersma B, Brethouwer G, Nieuwstadt F (1998) A numerical investigation on the effect of the inflow conditions on the self-similar region of a round jet. *Physics of fluids* 10(4):899–909
- Bowersox R, Schetz J (1994) Compressible turbulence measurements in a high-speed high-reynolds-number mixing layer. *AIAA Journal* 32(4):758–764, DOI 10.2514/3.12050
- Braza M, Perrin R, Hoarau Y (2006) Turbulence properties in the cylinder wake at high Reynolds numbers. *Journal of Fluids and Structures* 22(6-7):757–771, DOI 10.1016/j.jfluidstructs.2006.04.021
- Briassulis G, Agui J, Andreopoulos Y (2001) The structure of weakly compressible grid-generated turbulence. *Journal of Fluid Mechanics* 432:219–283, DOI 10.1017/s0022112000003402
- Bruun H (1996) *Hot-wire anemometry: principles and signal analysis*
- Chanal O, Chabaud B, Castaing B, Hébral B (2000) Intermittency in a turbulent low temperature gaseous helium jet. *European Physical Journal B* 17(2):309–317, DOI 10.1007/s100510070146
- Charonko J, Prestridge K (2017) Variable-density mixing in turbulent jets with coflow. *Journal of Fluid Mechanics* 825:887–921
- Chen S, Wang J, Li H, Wan M, Chen S (2018) Spectra and Mach number scaling in compressible homogeneous shear turbulence. *Physics of Fluids* 30(6), DOI 10.1063/1.5028294
- Danish M, Suman S, Girimaji S (2016) Influence of flow topology and dilatation on scalar mixing in compressible turbulence. *Journal of Fluid Mechanics* 793:633
- Davidson P, Kaneda Y, Sreenivasan K (2012) *Ten chapters in turbulence*. Cambridge University Press
- Donzis D, Jagannathan S (2013) Fluctuations of thermodynamic variables in stationary compressible turbulence. *Journal of Fluid Mechanics* 733:221–244, DOI 10.1017/jfm.2013.445



- Donzis D, John J (2019) Universality and scaling in compressible turbulence 1907.07871
- Federrath C (2013) On the universality of supersonic turbulence. *Monthly Notices of the Royal Astronomical Society* 436(2):1245–1257, DOI 10.1093/mnras/stt1644, 1306.3989
- Fellouah H, Ball C, Pollard A (2009) Reynolds number effects within the development region of a turbulent round free jet. *International Journal of Heat and Mass Transfer* 52(17-18):3943–3954, DOI 10.1016/j.ijheatmasstransfer.2009.03.029, URL <http://dx.doi.org/10.1016/j.ijheatmasstransfer.2009.03.029>
- Feng T, McQuirk J (2016) Measurements in the annular shear layer of high subsonic and under-expanded round jets. *Experiments in Fluids* 57(1):1–25, DOI 10.1007/s00348-015-2090-8
- Fleury V, Bailly C, Jondeau E, Michard M, Juve D (2008) Space-time correlations in two subsonic jets using dual particle image velocimetry measurements. *AIAA Journal* 46(10):2498–2509, DOI 10.2514/1.35561
- Freund J, Lele S, Moin P (2000) Compressibility effects in a turbulent annular mixing layer. Part 1. Turbulence and growth rate. *Journal of Fluid Mechanics* 421:229–267
- Gatski T, Bonnet J (2013) Compressibility, turbulence and high speed flow. Academic Press
- Georgiadis N, Yoder D, Vyas M, Engblom W (2014) Status of turbulence modeling for hypersonic propulsion flowpaths. *Theoretical and Computational Fluid Dynamics* 28(3):295–318, DOI 10.1007/s00162-013-0316-z
- Gilchrist R, Naughton J (2005) Experimental study of incompressible jets with different initial swirl distributions: Mean results. *AIAA Journal* 43(4):741–751, DOI 10.2514/1.3295
- Gloutak D (2018) Comparing compressibility effects in turbulence at various Mach numbers
- Griffin K, Wei N, Bodenschatz E, Bewley G (2019) Control of long-range correlations in turbulence. *Experiments in Fluids* 60(4):1–14, DOI 10.1007/s00348-019-2698-1, URL <http://dx.doi.org/10.1007/s00348-019-2698-1>, 1809.05126
- Gutmark E, Schadow K, Wilson K (1991) Effect of convective Mach number on mixing of coaxial circular and rectangular jets. *Physics of Fluids A* 3(1):29–36, DOI 10.1063/1.857860
- Honkan A, Andreopoulos J (1992) Rapid compression of grid-generated turbulence by a moving shock wave. *Physics of Fluids A* 4(11):2562–2572, DOI 10.1063/1.858443
- Hussein H, Capp S, George W (1994) Velocity measurements in a high-Reynolds-number, momentum-conserving, axisymmetric, turbulent jet. *Journal of Fluid Mechanics* 258:31–75, DOI 10.1017/S002211209400323X
- Hutchins N, Monty J, Hultmark M, Smits A (2015) A direct measure of the frequency response of hot-wire anemometers: temporal resolution issues in wall-bounded turbulence. *Experiments in Fluids* 56(1):1–18
- Iyer K, Sreenivasan K, Yeung P (2020) Scaling exponents saturate in three-dimensional isotropic turbulence. *Physical Review Fluids* 5(5):054605
- Jagannathan S, Donzis D (2016) Reynolds and Mach number scaling in solenoidally-forced compressible turbulence using high-resolution direct numerical simulations. *Journal of Fluid Mechanics* 789:669–707, DOI 10.1017/jfm.2015.754
- Jordan P, Colonius T (2013) Wave Packets and Turbulent Jet Noise. *Annual Review of Fluid Mechanics* 45(1):173–195, DOI 10.1146/annurev-fluid-011212-140756
- Karimi M, Girimaji S (2016) Suppression mechanism of kelvin-helmholtz instability in compressible fluid flows. *Physical review E* 93(4):041102
- Karimi M, Girimaji S (2017) Influence of orientation on the evolution of small perturbations in compressible shear layers with inflection points. *Physical Review E* 95(3):033112
- Kearney R, Bewley G (2020) Lagrangian tracking of colliding droplets. *Experiments in Fluids* 61(7):1–11

- King L (1914) XII . On the convection of heat from small cylinders in a stream of fluid: Determination of the convection constants of small platinum wires with applications to hot-wire anemometry. *Philosophical Transactions of the Royal Society A: Mathematical, Physical and Engineering Sciences* 214(509-522):373–432
- Kokmanian K, Scharnowski S, Bross M, Duvvuri S, Fu M, Kähler C, Hultmark M (2019) Development of a nanoscale hot-wire probe for supersonic flow applications. *Experiments in Fluids* 60(10):1–10, DOI 10.1007/s00348-019-2797-z
- Ladeinde F, Oh H (2021) Stochastic and spectra contents of detonation initiated by compressible turbulent thermodynamic fluctuations. *Physics of Fluids* 33(4), DOI 10.1063/5.0045293
- Lee S, Lele S, Moin P (1992) Simulation of spatially evolving turbulence and the applicability of Taylor’s hypothesis in compressible flow. *Physics of Fluids A* 4(7):1521–1530, DOI 10.1063/1.858425
- Lele S (1994) Compressibility Effects on Turbulence. *Annual Review of Fluid Mechanics* 26(1):211–254, DOI 10.1146/annurev.fluid.26.1.211
- Low MM, Klessen R (2004) Control of star formation by supersonic turbulence. *Reviews of Modern Physics* 76(1):125–194, DOI 10.1103/RevModPhys.76.125, 0301093
- Matsuno K, Lele S (2021) Internal regulation in compressible turbulent shear layers. *Journal of Fluid Mechanics* 907
- Murakami E, Papamoschou D (2002) Mean flow development in dual-stream compressible jets. *AIAA Journal* 40(6):1131–1138, DOI 10.2514/2.1762
- Mydlarski L, Warhaft Z (1996) On the onset of high-Reynolds-number grid-generated wind tunnel turbulence. *Journal of Fluid Mechanics* 320:331–368, DOI 10.1017/S0022112096007562
- Narayanan S, Barber T, Polak D (2002) High subsonic jet experiments: Turbulence and noise generation studies. *AIAA Journal* 40(3):430–437, DOI 10.2514/2.1692
- Owen F, Horstman C, Kussoy M (1975) Mean and fluctuating flow measurements of a fully-developed, non-adiabatic, hypersonic boundary layer. *Journal of Fluid Mechanics* 70(2):393–413, DOI 10.1017/S0022112075002091
- Pearson B, Krogstad P, Van De Water W (2002) Measurements of the turbulent energy dissipation rate. *Physics of Fluids* 14(3):1288–1290, DOI 10.1063/1.1445422
- Pitts W (1991) Reynolds number effects on the mixing behavior of axisymmetric turbulent jets. *Experiments in fluids* 11(2):135–141
- Pope S (2001) *Turbulent Flows*. DOI 10.1016/s0997-7546(01)01166-9
- Praturi D, Girimaji S (2019) Effect of pressure-dilatation on energy spectrum evolution in compressible turbulence. *Physics of Fluids* 31(5):055114
- Quadros R, Sinha K, Larsson J (2016a) Kovaszny mode decomposition of velocity-temperature correlation in canonical shock-turbulence interaction. *Flow, Turbulence and Combustion* 97(3):787–810
- Quadros R, Sinha K, Larsson J (2016b) Turbulent energy flux generated by shock/homogeneous-turbulence interaction. *J Fluid Mech* 796:113–157
- Rottländer H, Umrath W, Voss G (2016) *Fundamentals of leak detection*. Leybold (199)
- Ryu D, Kang H, Cho J, Das S (2008) Turbulence and magnetic fields in the large-scale structure of the universe. *Science* 320(5878):909–912, DOI 10.1126/science.1154923, 0805.2466
- Sabelnikov V, Lipatnikov A, Nishiki S, Dave H, Hernández Pérez F, Song W, Im H (2021) Dissipation and dilatation rates in premixed turbulent flames. *Physics of Fluids* 33(3), DOI 10.1063/5.0039101
- Samimy M, Zaman K, Reeder M (1993) Effect of tabs on the flow and noise field of an axisymmetric jet. *AIAA Journal* 31(4):609–619, DOI 10.2514/3.11594

- Samtaney R, Pullin D, Kosović B (2001) Direct numerical simulation of decaying compressible turbulence and shocklet statistics. *Physics of Fluids* 13(5):1415–1430, DOI 10.1063/1.1355682
- Sandberg R, Sandham N, Suponitsky V (2012) DNS of compressible pipe flow exiting into a coflow. *International Journal of Heat and Fluid Flow* 35:33–44, DOI 10.1016/j.ijheatfluidflow.2012.01.006, URL <http://dx.doi.org/10.1016/j.ijheatfluidflow.2012.01.006>
- Sarkar S, Lakshmanan B (1991) Application of a Reynolds stress turbulence model to the compressible shear layer. *AIAA Journal* 29(5):743–749, DOI 10.2514/3.10649
- Schadow K, Gutmark E, Wilson K (1990) Compressible spreading rates of supersonic coaxial jets. *Experiments in Fluids* 10(2-3):161–167, DOI 10.1007/BF00215025
- Schlichting H (1956) The Variable Density High Speed Cascade Wind Tunnel of the Deutsche Forschungsanstalt für Luftfahrt Braunschweig. Tech. Rep. 91
- Shandarin S, Zeldovich Y (1989) The large-scale structure of the universe: Turbulence, intermittency, structures in a self-gravitating medium. *Reviews of Modern Physics* 61(2):185–222
- Sinhuber M, Bodenschatz E, Bewley G (2015) Decay of turbulence at high reynolds numbers. *Physical review letters* 114(3):034501
- Slessor M, Zhuang M, Dimokatis P (2000) Turbulent shear-layer mixing: growth-rate compressibility scaling. *Journal of Fluid Mechanics* 414:35–45
- Spina E, Smits A (1987) Organized structures in a compressible, turbulent boundary layer. *Journal of Fluid Mechanics* 182(1962):85–109, DOI 10.1017/S0022112087002258
- Spina E, Smits A, Robinson S (1994) The physics of supersonic turbulent boundary layers. *Annual Review of Fluid Mechanics* 26(1):287–319, DOI 10.1146/annurev.fl.26.010194.001443
- Tang S, Antonia R, Djenidi L, Danaïla L, Zhou Y (2018) Reappraisal of the velocity derivative flatness factor in various turbulent flows. *Journal of Fluid Mechanics* 847:244–265, DOI 10.1017/jfm.2018.307
- Taylor G (1937) The statistical theory of isotropic turbulence. *Journal of the Aeronautical Sciences* 4(8):311–315
- Tennekes H, Lumley J (2018) A first course in turbulence. MIT press
- Urzay J (2018) Supersonic Combustion in Air-Breathing Propulsion Systems for Hypersonic Flight. *Annual Review of Fluid Mechanics* 50(1):593–627, DOI 10.1146/annurev-fluid-122316-045217
- Valente P, Vassilicos J (2012) Universal dissipation scaling for nonequilibrium turbulence. *Physical review letters* 108(21):214503
- Vanierschot M, Van den Bulck E (2008) Influence of swirl on the initial merging zone of a turbulent annular jet. *Physics of fluids* 20(10):105104
- Wang J, Shi Y, Wang L, Xiao Z, He X, Chen S (2011) Effect of shocklets on the velocity gradients in highly compressible isotropic turbulence. *Physics of Fluids* 23(12), DOI 10.1063/1.3664124
- Wang J, Shi Y, Wang L, Xiao Z, He X, Chen S (2012) Effect of compressibility on the small-scale structures in isotropic turbulence. *Journal of Fluid Mechanics* 713:588–631, DOI 10.1017/jfm.2012.474
- Wang J, Gotoh T, Watanabe T (2017) Spectra and statistics in compressible isotropic turbulence. *Physical Review Fluids* 2(1):1–26, DOI 10.1103/PhysRevFluids.2.013403
- Wang J, Wan M, Chen S, Xie C, Chen S (2018) Effect of shock waves on the statistics and scaling in compressible isotropic turbulence. *Physical Review E* 97(4):1–18, DOI 10.1103/PhysRevE.97.043108
- White C, Karpetsis A, Sreenivasan K (2002) High-Reynolds-number turbulence in small apparatus: Grid turbulence in cryogenic liquids. *Journal of Fluid Mechanics* 452:189–197, DOI 10.1017/S0022112001007194

- 
- Williams O, Sahoo D, Baumgartner M, Smits A (2018) Experiments on the structure and scaling of hypersonic turbulent boundary layers. *Journal of Fluid Mechanics* 834:237–270, DOI 10.1017/jfm.2017.712
- Wynanski I, Fiedler H (1969) Some measurements in the self-preserving jet. *Journal of Fluid Mechanics* 38(3):577–612, DOI 10.1017/S0022112069000358
- Yakhot V, Donzis D (2018) Anomalous exponents in strong turbulence. *Physica D: Nonlinear Phenomena* 384:12–17
- Zaman K (1998) Asymptotic spreading rate of initially compressible jets - Experiment and analysis. *Physics of Fluids* 10(10):2652–2660, DOI 10.1063/1.869778
- Zaman K (1999) Spreading characteristics of compressible jets from nozzles of various geometries. *Journal of Fluid Mechanics* 383:197–228, DOI 10.1017/S0022112099003833
- Zaman K, Steffen C, Reddy D (1997) Entrainment and spreading characteristics of jets from asymmetric nozzles. 4th Shear Flow Control Conference DOI 10.2514/6.1997-1878
- Zwart P, Budwig R, Tavoularis S (1997) Grid turbulence in compressible flow. *Experiments in Fluids* 23(6):520–522, DOI 10.1007/s003480050143